Electronic Supplementary Material (ESI) for Chemical Communications

Supporting Information

Multiple Fluorescence ΔCIE and ΔRGB Codes for Sensing Volatile Organic Compounds with a Wide Range of Response **

Kaijun Tian, Dehui Hu, Rui Hu, Shuangqing Wang, Shayu Li, Yi Li,* and Guoqiang Yang**

Experimental Section

General informations. All the chemicals are commercially available. Potassium t-butyl alcohol (98%) was obtained from Acros. Other chemicals were obtained from Beijing Chemical Reagents. All solvents were used after appropriate distillation or purification. 2,4,6-Trimethyl-s-triazine was synthesized according to the reference.[S1] ^{1}H-NMR and ^{13}C-NMR spectra were recorded on Bruker Avance 400 spectrometer. EI-MS spectrum was measured by SHIMADZU GC/MS-QP2010. HRMS was measured by ALLIANCE 2695/LCT PREMIER XE. UV-vis absorption spectra were recorded with a Hitachi U-3010 spectrophotometer. Photoluminescence spectra were carried out on a Hitachi F-4500 spectrophotometer. Elemental analyses were performed by Carlo Erba 1106. Photoluminescence spectra of the sensors were recorded with AvaSpec-2048 Standard Fiber Optic Spectrometer. Single-crystal X-ray crystallographic data for MQT was collected in Rigarku Raxis Rapid IP diffractometer.

Synthesis of the compounds:

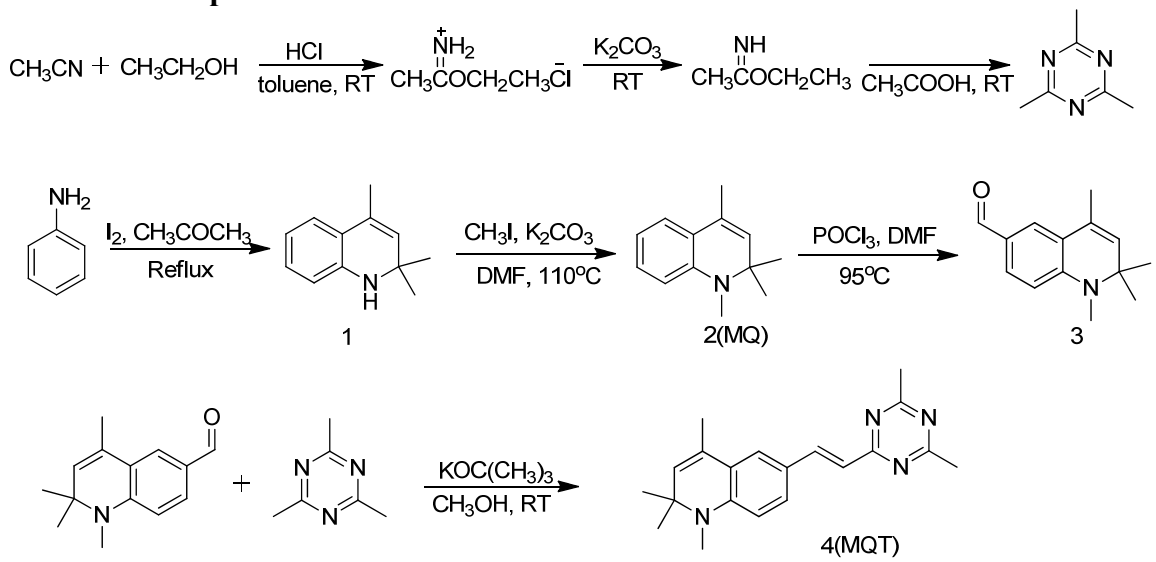

Scheme S1. Synthetic routes and chemical structures of the compounds.

2,2,4-Trimethyl-1,2-dihydroquinoline (1).

To the mixture of aniline (65.17 g) and iodine (3.24 g) was added dropwise acetone (180 ml) at 170 □ under dry argon. The water produced during the reaction was removed by distillation while keeping the rate of adding acetone in 1-2 drop(s) per second. The mixture was stirred at that temperature for 1 hour. Upon cooling to room temperature, the mixture was poured into water and extracted three times with ether. The combined organic layer was dried over magnesium sulfate. After removal of solvent, the product was purified by flash chromatography using hexane as eluent to give a yield of 64.5%. ^{1}H-NMR (400 MHz, $CDCl_3$): δ 7.06 (d, *J*=7.8 Hz, 1H), 6.94 (t, *J*=7.3 Hz, 1H), 6.59 (t, *J*=7.3Hz, 1H), 6.40 (d, *J*=7.8 Hz, 1H), 5.27 (s, 1H), 3.75 (br, 1H), 1.94 (s, 3H), 1.39 (s, 6H).

1,2,2,4-Tetramethyl-1,2-dihydroquinoline (MQ) (2).

The mixture of dihydroquinoline (1) (24.3 g), iodomethane (13.3 ml) and potassium carbonate (24.3 g) in 180 ml of DMF was heated at 110 □ under dry argon for 24 hours. Upon cooling to room temperature, the mixture was poured into water. The resultant mixture was extracted with ethyl ether. The combined organic layer was washed with water and dried over magnesium sulfate. After removal of solvent, the product was purified by flash chromatography using hexane/ethyl ether (100/1, v/v) as eluent to give a yield of 80.6%. ^{1}H-NMR (400 MHz, $CDCl_3$): δ 7.26 (t, *J*=7.8 Hz, 1H), 7.01 (d, *J*=8.0 Hz, 1H), 6.64 (t, *J*=7.4 Hz, 1H), 6.51 (d, *J*=8.1Hz, 1H), 5.28 (s, 1H), 2.77 (s, 3H), 1.97 (s, 3H), 1.27 (s, 6H).

1,2,2,4-Tetramethyl-1,2-dihydro-6-quinolinecarbaldehyde (3).

To a solution of 1,2,2,4-tetramethyl-1,2-dihydroquinoline (2) (9.77 g) in 150 ml of dry redistilled DMF was added phosphorus oxychloride (7.9 ml) dropwise at 0 □ under dry argon. The mixture was stirred at 95 □ overnight under dry argon. Upon cooling to room temperature, the mixture was poured into ice water (400 ml) and neutralized with aqueous solution of sodium hydroxide. Then the resultant mixture was extracted with ethyl ether, and the combined organic layer was washed with water and dried over anhydrous magnesium sulfate. After removal of solvent, the product was purified by flash chromatography using hexane/ethyl ether (100/5, v/v) as eluent to give a yield of 62.7%. ^{1}H-NMR (400 MHz, $CDCl_3$): δ 9.70 (s, 1H), 7.57 (d, *J*=8.4Hz, 1H), 7.53 (s, 1H), 6.52 (d, *J*=8.4Hz, 1H), 5.31 (s, 1H), 2.91 (s, 3H), 2.02 (s, 1H), 1.38 (s, 6H).

Stilbene-2,4-dimethyl-6-(1,2,2,4-tetramethyl-1,2-dihydroquinolin-6-yl)-1,3,5-s-triazine (MQT) (4).

To a solution of 1,2,2,4-tetramethyl-1,2-dihydro-6-quinolinecarbaldehyde (3) (2.15 g) in dry MeOH (20 ml) was added slowly at 0 □ to a solution of 2,4,6-trimethyl-s-triazine (1.23 g) and $KOC(CH_3)_3$ (1.68 g) in dry MeOH (100 ml). After vigorous stirring for 30 min, the reaction mixture was kept at room temperature overnight. The volatile parts were removed and the residue was purified by column chromatography using CH_2Cl_2/ethyl acetate (5/1, v/v) as eluent to give a yield of 48.2%. ^{1}H-NMR (400 MHz, $CDCl_3$): δ 8.14 (d, *J*=16Hz, 1H), 7.39 (s, 1H), 7.36 (s, 1H), 6.84 (d, *J*=16Hz, 1H), 6.50 (d, *J*=8Hz, 1H), 5.31 (s, 1H), 2.87 (s, 3H), 2.61 (s, 6H), 2.01 (s, 3H), 1.35 (s, 6H). ^{13}C-NMR (100 MHz, $CDCl_3$): δ 175.71, 171.85, 147.30, 143,34, 130.67, 130.15, 127.61, 123.20, 123.12, 122.73, 119.85, 110.34, 57.24, 31.11, 28.38, 25.87, 18.80. EI-MS (m/z): $[M]^+$ calcd for $C_{20}H_{24}N_4$ 320.2, found 320. HRMS (m/z): $[M+H]^+$ calcd. for $C_{20}H_{25}N_4^+$ 321.2079, found 321.2065. Anal. Calcd. for $C_{20}H_{24}N_4$: C, 74.97; H, 7.55; N, 17.48, found: C, 74.89, H 7.64, N, 17.44.

X-ray crystallographic data of MQT

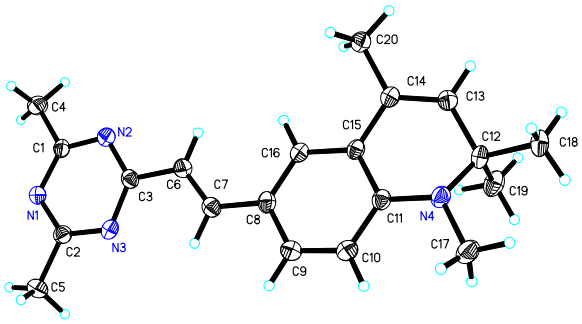

Figure S1. X-ray crystallographic structure of MQT.

In the MQ donor, the nitrogen atom is locked to diminish the probability of the nonradiative transition. This is illustrated in the crystal structure. Mean values of the C-N-C bond angle in the donor is 117.6 and N (4), C (11), C (17) are in same plane of the whole molecule, except that C (12) have a little deviation from the plane. This indicates that the p orbit of the N (4) has stronger intramolecular p-π interactions with its adjacent phenyl rings than the N, N-diethylamine counterpart, which facilitates ICT. Consequently, the excitation of the ICT state will accompany with a charge transfer from the MQ donor to the triazine acceptor.

Table S1. Crystallographic Data and Refinement Details for MQT.

Compound Empirical formula	$C_{20}H_{24}N_4$
Crystal colour	Yellow
Formula wt.	320.43
Temperature (K)	173(2)
Wavelength (Å)	0.71073
Crystal system	Monoclinic
Space group	P2(1)/c
Unit cell dimensions	*a*=13.828(2) Å α=90 deg.
	b=15.610(4) Å β=95.70(4) deg.
	c=8.175(4) Å γ=90.00 deg.
Volume (Å^3)	1755.8(10)
Z	4
Density (calculated, g/cm^3)	1.212
F_{000}	688
Crystal dimensions (mm)	0.47 x 0.40 x 0.13
θ range for data collection (deg.)	2.82 to 25.00
Ranges of *h, k, l*	-16<=h<=16, -17<=k<=18, -8<=l<=9
Reflections collected	Total: 11603
	Unique: 3056 (R_{int} = 0.0341)
Refinement method	Full-matrix least-squares on F^2
Absorption correction	Numerical
Max. and min. transmission	0.9905 and 0.9662
Data / restraints / parameters	3056/0/ 223
Goodness-of-fit on F^2	1.115
Final R indices (I>2σ(I))	R1 = 0.0948, wR2 = 0.2475
R indices (all data)	R1 = 0.0977, wR2 = 0.2495
Absorption coefficient(mm^{-1})	0.074
Largest diff. peak and hole e$^-$/ Å^3	0.371 and -0.243

$R_1 = \Sigma||F_o| - |F_c||/\Sigma|F_o|$, $wR_2 = [\Sigma w(F_o^2 - F_c^2)^2/\Sigma w(F_o^2)^2]^{1/2}$

Table S2. Atomic coordinates and equivalent isotropic displacement parameters of $C_{20}H_{24}N_4$.

atom	x	y	z	U(eq)
N(1)	0.0696(2)	0.2147(2)	0.7572(4)	0.0036(1)
N(2)	0.2068(2)	0.1596(2)	0.6380(4)	0.0038(1)
N(3)	0.1782(2)	0.3097(2)	0.6397(4)	0.0036(1)
N(4)	0.6786(2)	0.4210(2)	0.1550(4)	0.0038(1)
C(1)	0.1279(3)	0.1513(2)	0.7172(5)	0.0035(1)
C(2)	0.0979(3)	0.2931(2)	0.7140(5)	0.0036(1)
C(3)	0.2299(3)	0.2406(2)	0.6035(4)	0.0035(1)
C(4)	0.1031(3)	0.0623(3)	0.7681(6)	0.0048(1)
C(5)	0.0359(3)	0.3664(3)	0.7527(6)	0.0049(1)
C(6)	0.3182(3)	0.2522(2)	0.5214(5)	0.0038(1)
C(7)	0.3467(3)	0.3285(3)	0.4716(4)	0.0037(1)
C(8)	0.4317(3)	0.3486(2)	0.3879(4)	0.0037(1)
C(9)	0.4460(3)	0.4333(3)	0.3404(5)	0.0043(1)
C(10)	0.5258(3)	0.4580(3)	0.2643(5)	0.0043(1)
C(11)	0.5971(3)	0.3985(2)	0.2328(4)	0.0034(1)
C(12)	0.7687(3)	0.3714(2)	0.1964(5)	0.0036(1)
C(13)	0.7422(3)	0.2776(2)	0.1968(4)	0.0037(1)
C(14)	0.6567(3)	0.2486(2)	0.2365(4)	0.0034(1)
C(15)	0.5842(2)	0.3115(2)	0.2758(4)	0.0031(1)
C(16)	0.5015(3)	0.2884(2)	0.3510(4)	0.0034(1)
C(17)	0.6878(3)	0.5106(3)	0.1079(6)	0.0052(1)
C(18)	0.8399(3)	0.3849(3)	0.0647(5)	0.0046(1)
C(19)	0.8184(3)	0.3974(3)	0.3651(5)	0.0050(1)
C(20)	0.6331(3)	0.1547(2)	0.2404(5)	0.0038(1)

U_{eq} is defined as one third of the trace of the orthogonalized U_{ij} tensor.

Table S3. Selected Bond lengths (Å) and angles [deg] of $C_{20}H_{24}N_4$.

Bond	Distance	Atom	Angle
N(4)-C(11)	1.392(5)	C(11)-N(4)-C(17)	117.3(3)
N(4)-C(17)	1.459(5)	C(11)-N(4)-C(12)	117.7(3)
N(4)-C(12)	1.478(5)	C(17)-N(4)-C(12)	117.9(3)

Spectra of MQT:

Most polarity dyes undergo intramolecular charge transfer upon excitation and typically has a larger dipole moment in the excited state (μ_e) than in the ground state (μ_g). On absorption of a photon by the fluorophore, redistribution of electrons occurs in a very short time (10^{-15}s), a time too short for the displacement of nuclei or solvent cage. This results in an almost instantaneous change in the dipole moment. Following excitation, the solvent cage undergoes relaxation or reorganization around μ_e, leading to a relaxed state of minimum free energy.

The absorbing molecule is exposed to the same local environment in the ground and excited states. In contrast, the emitting fluorophore is exposed to the relaxed environment, which contains solvent molecules oriented around the dipole moment of the excited state. Therefore, emission is more sensitive to solvent polarity than absorption. The higher the polarity of the solvent, the lower the energy of the relaxed state and the larger the red-shift of the emission spectrum.[S2]

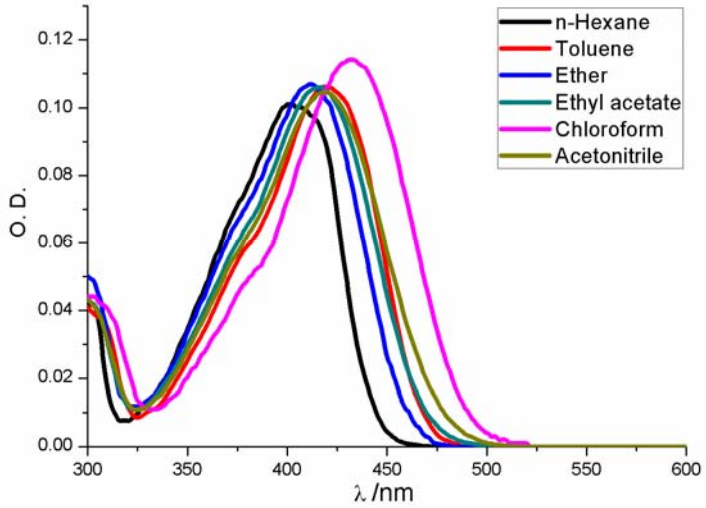

Figure S2. UV/Vis absorption spectra of MQT (3.0×10^{-6} M) in six solvents at 20°C.

As a result of less chance of nonradiative decay, the fluorescence quantum yield (η) of MQT is significantly enhanced (about 14 times), relative to the dialkylamino counterpart.[S3] From nonpolar solvent to polar solvent, the emissions maxima with more than 100nm shift are more sensitive to solvent than the absorption maxima with about 30nm shift. And stokes shift of MQT is very large and increases as solvent polarity increases, indicating the efficient process of ICT. Moreover, the η is significantly enhanced from nonpolar solvent to polar solvent, which endows the resulting sensor array with a wide range of response. This was the so-called "negative solvatokinetic effect", which was explained by several mechanisms such as biradicaloid charge transfer, proximity effect, and conformational changes.[S4] As a result, the η can be significant improved by the enhanced population of an emissive CT state in the polar solvent.

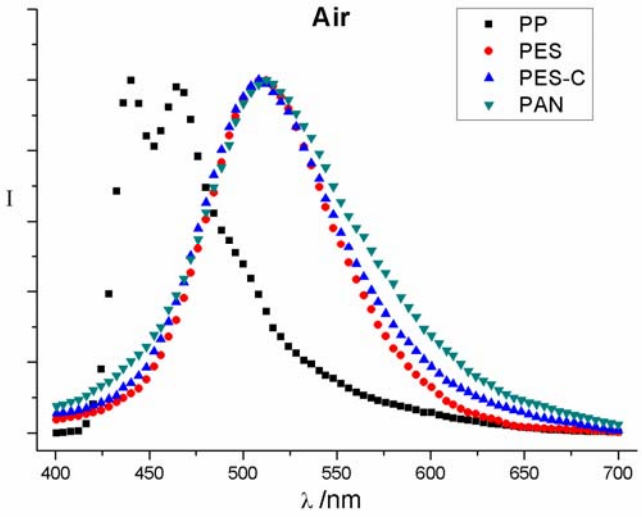

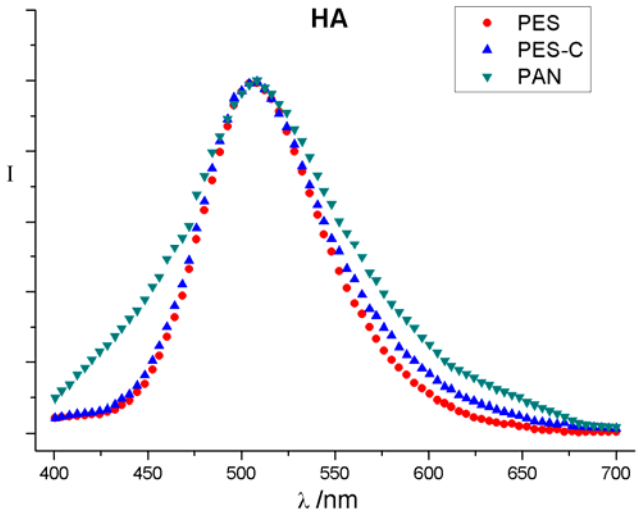

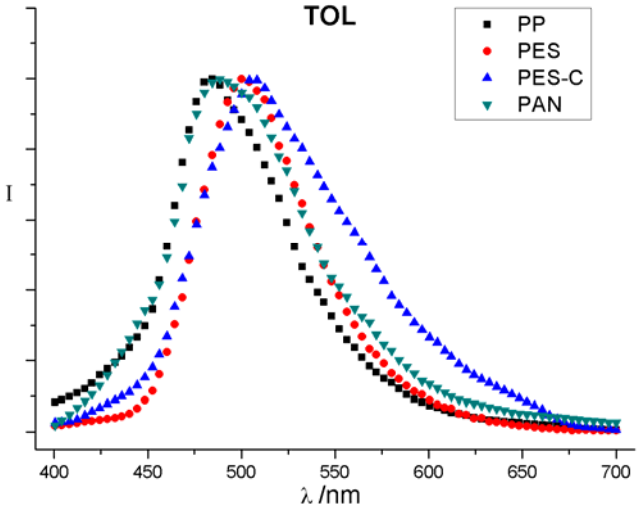

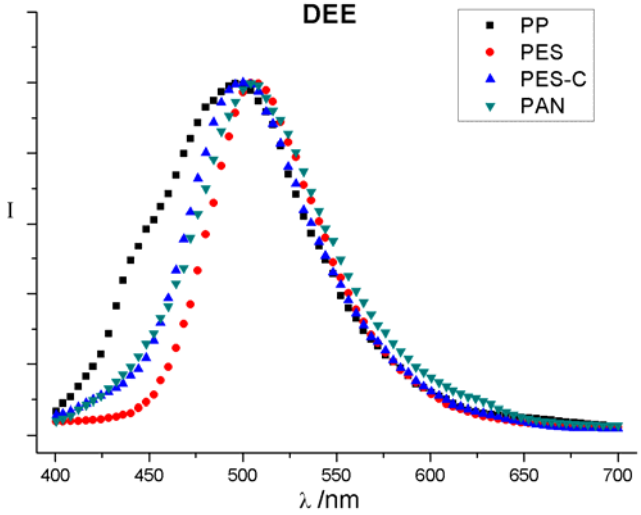

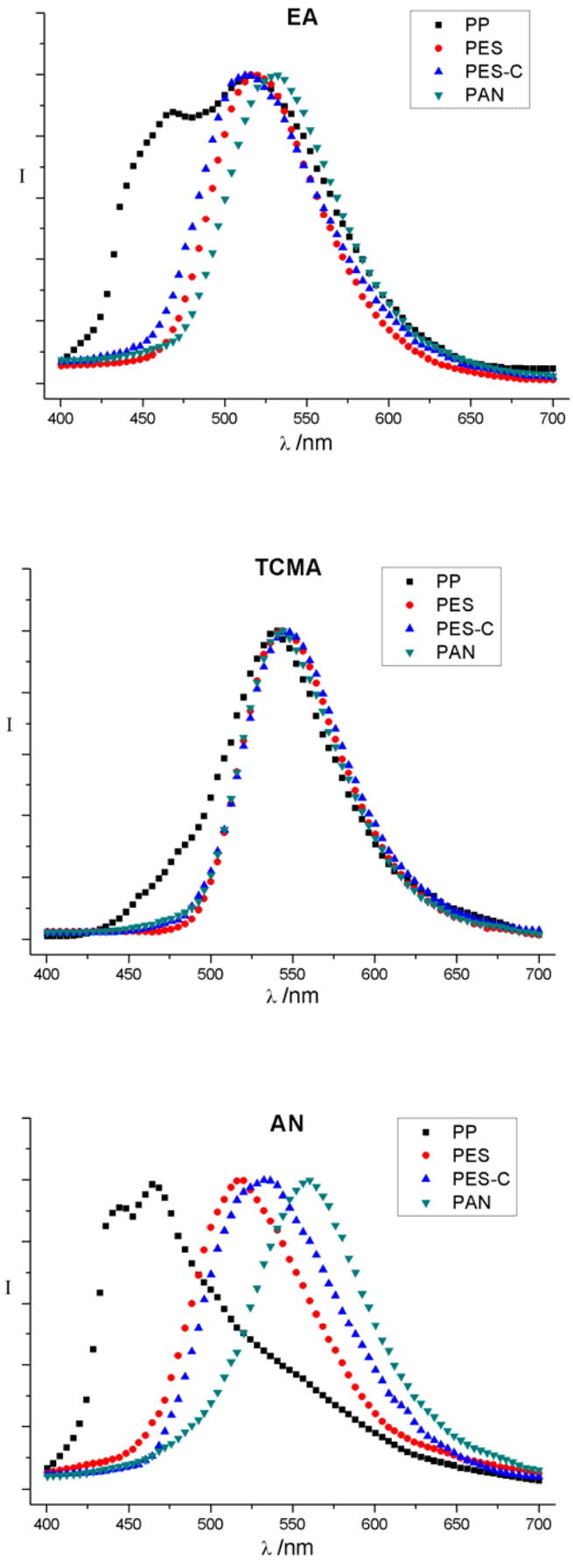

Figure S3. Luminescence spectra of sensor array in air and six representative VOCs.

Table S4. Summary of digital database of CIE coordinates for VOCs.

	PP	PES	PES-C	PAN
Air	(0.168, 0.160)	(0.219, 0.485)	(0.240, 0.465)	(0.266, 0.457)
HA		(0.209, 0.477)	(0.231, 0.467)	(0.246, 0.409)
TOL	(0.177, 0.335)	(0.197, 0.477)	(0.268, 0.473)	(0.205, 0.374)
DEE	(0.193, 0.327)	(0.218, 0.501)	(0.206, 0.416)	(0.225, 0.433)
EA	(0.234, 0.362)	(0.259, 0.553)	(0.261, 0.510)	(0.299, 0.552)
TCMA	(0.324, 0.542)	(0.367, 0.585)	(0.371, 0.574)	(0.359, 0.577)
AN	(0.211, 0.247)	(0.280, 0.518)	(0.327, 0.545)	(0.394, 0.518)

Table S5. Summary of ΔR, ΔG, ΔB before and after exposure to VOCs.

	PP/ΔR	PP/ΔG	PP/ΔB	PES/ΔR	PES/ΔG	PES/ΔB
HA	2	-16	-23	-1	65	41
TOL	0	-4	-21	-1	27	16
DEE	0	25	10	-1	23	10
EA	0	9	-13	-1	42	6
TCMA	11	11	-36	28	29	-22
AN	2	4	-4	2	48	11
	PES-C/ΔR	PES-C/ΔG	PES-C/ΔB	PAN/ΔR	PAN/ΔG	PAN/ΔB
HA	-1	79	47	-1	7	14
TOL	-1	41	19	-1	11	25
DEE	-1	22	23	-1	27	24
EA	-1	60	21	-1	80	17
TCMA	41	47	-22	24	24	-11
AN	17	41	-11	21	-15	-20

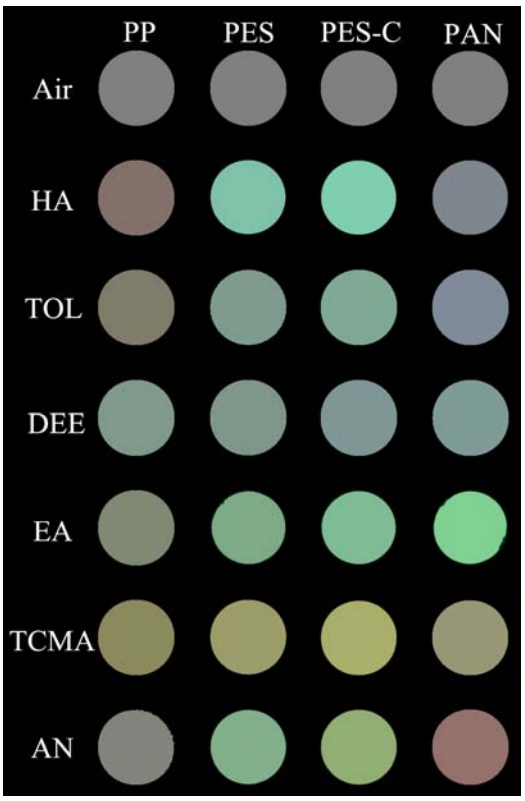

Figure S4. Intuitive images of ΔRGB with 50% gray as starting point.

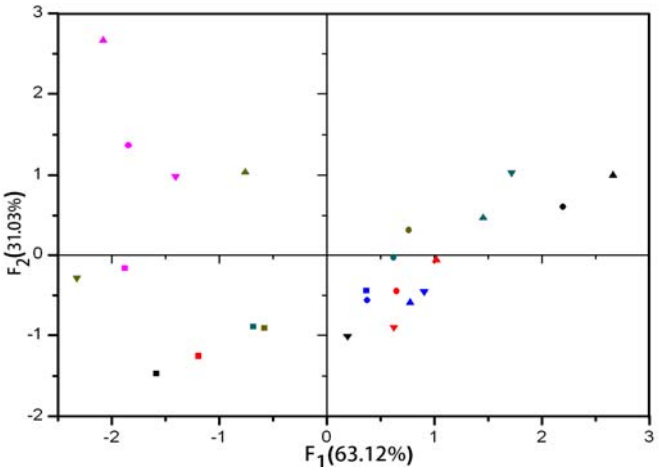

Fig. S5. Principal component analysis plot of MQT-sensors responses upon exposure to the six analytes. For each data point, the shapes represent polymer substrates (■: PP, ●: PES, ▲: PES-C, ▼: PAN) and the colors represent VOCs (Black: HA, Red: TOL, Blue: DEE, Dark Cyan: EA, Magenta: TCMA, Dark Yellow: AN).

The first two components account for 94.15% of the variance and are therefore used. The magenta cluster and yellow cluster, represented TCMA and AN, are far separated from the other clusters. The data for HA vapor also show large spread in the component values. These results suggest that the array is high response to the TCMA, AN, and HA vapor recognition. Some cluster points of other three solvents are located relatively close to each other, but at least one point for each analyte is clearly discernible.

Motivated by the favorable ΔCIE/ΔRGB changes observed in preliminary experiments, we took a step toward the potential use of the sensor array for the detection of low concentration VOC in air. TCMA is widely used in industry and presents in our environment. A short-time exposure to above 900 ppm TCMA causes dizziness, fatigue, and headache.13 In our practical test, the sensor array was exposed to TCMA within 300s at 500 ppm (IDLH concentration: Immediately Dangerous to Life or Health concentration). A moderate colorimetric change can be observed with naked eyes. The corresponding ΔCIE vectors, (-0.010, 0.027), (0.009, 0.040), (0.007, 0.061), (-0.003, 0.017), are large enough to be readily measured by colorimeter.

Reference

(S1) Schaefer, F. C.; Peters, G. A. *J. Org. Chem.* **1961**, *26*, 2778-2784.

(S2) Lakowicz, J. R. *Principles of Fluorescence Spectroscopy (Third Edition)*, Springer Press, New York, **2006**, p. 206.

(S3) Cui, Y. Z.; Fang, Q.; Huang, Z. L.; Xue, G.; Xu, G. B.; Yu, W. T. *J. Mater. Chem* **2004**, *14,* 2443–2449.

(S4) Rurack, K.; Dekhtyar, M. L.; Bricks, J. L.; Resch-Genger, U.; Rettig, W. *J. Phys. Chem. A* **1999,** *103,* 9626-9635.